Regulation of the activity in the p53 family depends on the organization of the transactivation domain

Katharina Krauskopf[1,4], Jakob Gebel[1,4], Sina Kazemi[1], Marcel Tuppi[1], Frank Löhr[1], Birgit Schäfer[1], Joachim Koch[2], Peter Güntert[1], Volker Dötsch[1,5*] and Sebastian Kehrloesser[1,3*]

[1]Institute of Biophysical Chemistry and Center for Biomolecular Magnetic Resonance Goethe University, Frankfurt/Main, Germany

[2]Georg-Speyer-Haus, Frankfurt/Main, Germany

[3]current address: Cancer Research UK, Cambridge Institute, University of Cambridge, Cambridge CB2 0RE, United Kingdom

[4]These authors contributed equally to this work

[5]Lead Contact

*Correspondence: vdoetsch@em.uni-frankfurt.de (V.D.), sebastian.kehrloesser@cruk.cam.ac.uk (S.K.)

Summary

Despite high sequence homology among the p53 family members, the regulation of their transactivation potential is based on strikingly different mechanisms. Previous studies revealed that the activity of TAp63α is regulated via an autoinhibitory mechanism that keeps inactive TAp63α in a dimeric conformation. While all p73 isoforms are constitutive tetramers, their basal activity is much lower compared to tetrameric TAp63. We show that the dimeric state of TAp63α not only reduces DNA binding affinity, but also suppresses interaction with the acetyltransferase p300. Exchange of the transactivation domains is sufficient to transfer the regulatory characteristics between p63 and p73. Structure determination of the transactivation domains of p63 and p73 in complex with the p300 Taz2 domain further revealed that in contrast to p53 and p73, p63 has a single transactivation domain. Sequences essential for stabilizing the closed dimer of TAp63α have evolved into a second transactivation domain in p73 and p53.

Keywords:
p63 / p73 / p53 family / p300 / oligomerization

Introduction

The three p53 family members p53, p63 and p73 play major roles in developmental processes, tumor suppression and in the surveillance of genetic stability. Knock out mouse studies have revealed a role of p63 in the development of the epidermis and in quality control in oocytes (Yang et al., 1999, Mills et al., 1999, Suh et al., 2006). This quality control in germ cells is most likely the most ancient function of the entire protein family since even invertebrates such as *C. elegans* and *D. melanogaster* express p63-like proteins in their germ cells (Derry et al., 2001, Ollmann et al., 2000). In mice p63 and p73 are expressed as several different isoforms created by the combination of different promoters and processing by C-terminal splicing (Yang et al., 1998). The longest p63 isoform, TAp63α, is highly expressed in primary oocytes that are arrested in prophase of meiosis I. In humans, oocytes enter the dicyate arrest phase around birth. This phase lasts until oocytes get recruited for ovulation, which can last up to 50 years (start of menopause). During this long arrest time the high cellular concentration of TAp63α ensures that the genetic quality of the germ cells is maintained through a TAp63α dependent induction of apoptosis triggered by detection of DNA damage. This quality control mechanism can have drastic consequences for female cancer patients treated with chemotherapeutic drugs. As these drugs inflict DNA damage they indirectly activate TAp63α resulting in the elimination of compromised oocytes (Gebel et al., 2017). As females are born with a finite number of oocytes, their loss results in infertility and the premature induction of menopause including loss of ovarian endocrine functions (Woodard and Bolcun-Filas, 2016). To prevent loss of oocytes under normal circumstances, the activity of TAp63α is very tightly regulated. We could show that in arrested oocytes TAp63α adopts a closed and only dimeric conformation (Deutsch et al., 2011). Inhibition is based on the formation of a six-stranded anti-parallel β-sheet created from one β-strand of the C-terminal transactivation inhibitory domain (TID) (Serber et al., 2002) and two β-strands from the N-terminal region which blocks the tetramerization interface of the tetramerization domain (Coutandin et al., 2016). Detection of DNA damage initiates a kinase cascade that leads to a sequential phosphorylation of TAp63α by Chk2 (Bolcun-Filas et al., 2014) and CK1 triggering the formation of an open and tetrameric state (Tuppi et al., 2018). This open tetrameric conformation has a twentyfold higher DNA binding affinity compared to the closed dimeric conformation (Suh et al., 2006, Deutsch et al., 2011). Given the importance of germ cells as basically immortal cells that are the source of germ cells for all following generations, it is likely that additional mechanisms ensure that the limited number of oocytes is not diminished by accidental activation of apoptosis. Such an additional mechanism could include preventing interaction of TAp63α with the transcriptional machinery. In previous studies we have indeed shown that the N-terminal helical transactivation domain binds to the central oligomerization domain (Deutsch et al., 2011). Here we show that the interaction with

the transcriptional machinery is strongly reduced in the dimeric state. Our analysis demonstrates that sequences that are important to stabilize the closed dimeric state in p63 have been converted into parts of the transactivation domain in the constitutively tetrameric family members p73 and p53. Through structure determination we finally demonstrate that the interaction between the p63 transactivation domain and the p300 Taz2 domain is different from the respective interactions of the p53 and p73 transactivation domains and does not require further posttranslational modifications for high affinity binding.

Results

Many regulators of critical cellular functions use autoinhibitory mechanisms. To create a switch-like function their activity is often controlled by two independent inhibitory mechanisms. Through such a combination the total inhibitory effect is the product of the inhibition efficiency of both processes, making a very tight regulation possible. Examples are N-WASP (Prehoda et al., 2000) involved in initiating actin polymerization and the guanine nucleotide exchange factor Vav1 (Yu et al., 2010). Previously we have shown that adopting the closed dimeric conformation inhibits the DNA binding affinity of TAp63α twentyfold (Deutsch et al., 2011). However, we could also show that the N-terminal helical transactivation domain binds back to the oligomerization domain and stabilizes the closed dimer. This interaction requires the three hydrophobic residues F16, W20 and L23, which in the transactivation domain of p53 are crucial for interaction with Mdm2. Mutating, these three amino acids to alanines in TAp63α results in the disruption of the closed conformation and the formation of an open tetramer. However, mutating these three amino acids makes TAp63α transcriptionally inactive, despite its open conformation and demonstrates the importance of these residues. Based on these observations we predicted that in addition to DNA binding also the interaction with the transcriptional machinery is inhibited in the closed inactive state and hence total inhibition is the result of these two different mechanisms. To test this hypothesis we performed pulldown experiments of TAp63α with the Taz1 and Taz2 domains of the co-activator p300. Almost no interaction could be detected while the constitutively open and tetrameric isoform TAp63γ showed strong interaction with both domains (Figure 1). Comparison with the highly homologous family member p73 showed that neither TAp73α nor TAp73β interact strongly, despite both being constitutively open tetramers.

The low binding affinity seen in the pulldown experiments with p73 correlates with our previous investigation showing that despite being constitutive tetramers all p73 isoforms are far less transcriptionally active than their corresponding tetrameric p63 homologs (Luh et al.,

2013). To investigate if the low transcriptional activity is indeed a characteristic of the TA domain we measured the activity of chimeras of TAp73β (Figure 2A) containing either the DNA binding domain (DBD), the tetramerization domain (TD) or the TA domain of p63 (Figure 2B). Only the exchange of exon1 and exon2 to (amino acids 2-69) resulted in a significant increase in transcriptional activity, reaching that of the constitutively active TAp63γ isoform (Figures 2C and S1A-C). These results suggested that the TA domain of p63 has an inherently high transactivation potential. Consistent with this interpretation, a chimera of TAp63γ with the transactivation domain of p73 shows low transcriptional activity despite its open and tetrameric state (Figure S1D).

These experiments show three important principles of the regulation of p63 and p73: 1) The inhibitory mechanism of TAp63α includes two different mechanisms. In addition to inhibiting the DNA binding activity, the closed conformation suppresses the interaction with the transcriptional machinery. 2) The high transcriptional activity of the p63 transactivation domain paired with the high concentration of TAp63α in resting oocytes makes regulation of the activity through the oligomeric state very efficient. While the closed dimeric state shows no activity, the open tetrameric state has high transcriptional activity. 3) Despite their open tetrameric state TAp73 isoforms require further mechanisms such as posttranslational modifications to reach strong transcriptional activity.

To further investigate the different modes of regulation of p63 and p73 we decided to characterize the interaction between both transactivation domains and p300 in more detail.

The decisive difference between the TA domain of p63 and its mammalian homologs is its structural organization

For a more detailed investigation the boundaries of the transactivation domains had to be identified first. Structural and functional analyses of the transactivation domains of p53 and p73 have suggested that both are divided into two separate domains, TA1 and TA2 (Burge et al., 2009, Krois et al., 2016). In the transactivation domain of p63 the two stretches of amino acids corresponding to TA1 and TA2 have been assigned to 1-29 and 30-67. The sequence 30-67, however, had been identified in our previous investigations as forming two β-strands as part of the inhibitory β-sheet that keeps TAp63α in the closed, dimeric conformation (Coutandin et al., 2016). To validate the importance of both sequence stretches for the transcriptional activity, we mutated key hydrophobic residues in the TA1 and TA2 domains of all three family members and measured the transactivation potential on the p21 promoter in Saos2 cells. For p53 mutating the hydrophobic motifs (F19, W23, L26 in TA1 or I50, W53, F54 in TA2) led to an almost complete loss of the transcriptional activity (Figures 3A and S1E). Similarly, mutating the F15, W19, L22 motif in TA1 resulted in a reduction of p73 to almost background levels (Figures 3A and S1E). Mutation of the hydrophobic motif (F16,

W20, L23) in the TA domain of TAp63γ resulted in the expected total loss of activity. However, mutating key hydrophobic motifs (I33, L35 F37 or I50, I52, M54) in the sequence that corresponds to the TA2 domains in p53 and p73 had only minor effects (Figures 3A and S1E), suggesting that this sequence plays a minor role in transactivation but is required for the inhibitory mechanism in the TAp63α isoform. These results are also consistent with the transcriptional activity of chimeric proteins of TAp73β with either exon1 (amino acids 2-25) or exon1 and 2 (amino acids 2-69) of p63. Both chimeras reach high transactivation potential comparable to TAp63γ, suggesting that the sequence stretch 30-69 in p63 does not further contribute to transcriptional activity.

Further dissection of the transactivation domain showed that the full p63-like transcriptional activity could be observed by exchanging the first part of exon1, corresponding to amino acids 2 to 15 (Figures 3C and S1F). The high sequence identity of the TA domains between p63 and p73 of the first seven amino acids allowed the conclusion that amino acids 8 to 15 confer the high transactivation potential of TAp63, which we could confirm with the corresponding chimera (Figures 3C and S1F).

This interpretation is further supported by a comparative sequence analysis: amino acids 10 to 14 of p63 show the highest sequence identity to the N-terminal part of TA2 of p53 (Figure 3B). This analysis further supports the interpretation that p63 contains only one transactivation domain spanning amino acids 8 to 25 that combines elements of the p53 TA1 and TA2 domains.

To investigate these interactions quantitatively we measured the binding affinities of peptides derived from the TA domains to the Taz2 domain of p300 using fluorescence anisotropy. We chose the Taz2 domain because it displays the highest affinity of all p300 domains for the TAs of p53 and p73 (Burge et al., 2009, Krois et al., 2016). The affinity of a p63 peptide spanning amino acids 8-32 to the Taz2 domain was about five times higher (K_D = 0.19±0.02 μM, Figure 3D) than observed for the corresponding p73 peptide (K_D = 0.94±0.06 μM, Figure 3D). These data are consistent with the low affinity of p73 seen in the pulldown assays and with the low transcriptional activity. Exchanging amino acids 8-15 of p73 to those of p63 led to an increase in affinity reaching the value of the p63 TA (K_D = 0.12±0.01 μM, Figure 3D).

The TA domains of p63 and p73 use different binding sites on the p300 Taz2 domain

To further understand differences and similarities between the TA domains of p63 and p73 we solved the solution structures of both peptides in complex with the Taz2 domain of p300. Since the isolated p63 and p73 peptides are in intermediate exchange on the NMR time scale resulting in broad resonances (similar to the p53 peptides (Krois et al., 2016); Figure S2), we fused the peptides covalently to the Taz2 expression construct. Structures of

the TA1 and TA2 domains of p53 in complex with the CBP Taz2 and Taz1 domains have been solved before. These structures showed that both p53 peptides adopt different conformations and bind in an orthogonal manner with respect to each other (Miller Jenkins et al., 2015, Feng et al., 2009). In a recent study (Krois et al., 2016), however, the structures of a combined TA1-TA2 peptide covalently attached to Taz2 or Taz1 were solved, showing how both transactivation domains contribute to binding with most of the binding energy being contributed by TA2.

As predicted by our sequence analysis the p63 TA forms a single long helix that combines sequence elements of both p53 TA1 and TA2. The p63 TA and p53 TA2 share a similar orientation on the surface of the Taz2 domains (Figure 4B, F), albeit at an angle of ~26°. They both bind to the hydrophobic surface formed by helices 1-3 of the Taz2 domain. The helix formed by the p63 TA is longer by one turn at the C-terminus due to two additional hydrophobic interactions (F22, L23), which are not present in p53 TA2. However, a structural alignment of p53 TA2 and p63 TA (Figure 4A) revealed that although the general amphipathicity of both helices is conserved several amino acids are different. For example, W53 of p53 corresponds to the smaller I19 in p63, whereas F54 of p53 is replaced by the larger W20 of p63. The partial backbone assignment of a longer Taz2-p63 construct (up to amino acid D82) revealed no additional secondary structure elements (Figure S2) indicating that unlike p53 and p73, p63 has no dipartite transactivation domain, confirming our analysis described above.

For structure determination of the p73 TA bound to the Taz2 domain we initially used the peptide D10 – L67 as reported by Burge et al. (Burge et al., 2009) (assigned BEST-TROSY: Figure S3). The resulting structure confirmed the separation of the transactivation domain into a TA1 (15-29) and a TA2 (61-65) subdomain (Figure S3). However, the TA2 subdomain does not produce assignable long-range NOE contacts to the Taz2 domain, making it impossible to define its binding site. Therefore, we used a shorter construct, leading to a significant increase in protein stability as well as a reduction of signal overlap (assigned BEST-TROSY: Figure S3). The TA1 subdomain shows a virtually identical secondary structure in both constructs based on TALOS prediction (Figure S3) as well as NOE contacts. Thus, it can be assumed that the position of the p73 TA1 is correct and not influenced by the presence of TA2. A likely candidate for the interaction surface of the TA2 is the secondary low affinity binding site, which has been shown to bind p53 TA1 in the case of the combined p53 TA1-TA2 peptide (Krois et al., 2016).

The p73 TA1 adopts a different conformation on the Taz2 compared to structures of other transactivation domains (Figure 4). The classical Mdm2 binding motif (F15 to L22 (Kussie et al., 1996)) forms a helix. In contrast to p53 TA2 and p63 TA, however, the helix is not situated directly on top of helices 1-3 of Taz2. In addition to this helix p73 features two

aromatic residues (Y28 and F29), which are involved in Taz2 binding and are buried deeply in the groove that is normally occupied by the tryptophan residue of p53 TA2 or p63 TA. Mutation of those residues to alanine does not completely abolish binding to Taz2 but the binding affinity is significantly decreased (K_D > 50μM, Figure S3).

Exchange of the TA domains changes the oligomeric state of the α-isoforms

The results of our functional and structural analysis of the TAs of p63 and p73 have revealed that the structural organization of the TA is a decisive difference between both proteins. Exchanging the TA-domain of p73 with the one of p63 confers the high transcriptional activity of p63. We wondered if this transfer of the TA domain could also confer the ability to form a closed dimeric state to p73. To investigate this question we created a chimera of full length TAp73α containing exon1 and exon2 of p63. This construct includes in addition to p63's TA domain (8-25) the ILF (I33, L35 F37) and IIM (I50, I52, M54) motifs that together with the C-terminal TID form the inhibitory β-sheet. Exchanging exon1 and exon2 indeed created a closed and dimeric TAp73α chimera while exchanging only exon1 (amino acids 2 to 25), which lacks the ILF and IIM motifs, was not sufficient to change the oligomeric state of TAp73α (Figures 5A, B and S4B-D). We also created a TAp63α chimera containing the p73 TA (amino acids 2 to 25). This chimera forms a closed dimeric structure underscoring the importance of the ILF and IIM motifs and shows that the p73 TA1 can support the closed state (Figures 5C and S4A, E).

As controls we replaced the TID (amino acids 553 to 636) in TAp63α with the corresponding p73 sequence, which did not change the oligomeric state (Figures 5D and S4A, F). The exchange of the TD (including the linker between DBD and TD) destabilized the dimeric conformation (Figures 5E and S4A, G), while replacing the TA (amino acids 2-96) with the corresponding p73 sequence disrupted the closed dimeric state resulting in an open tetrameric profile (Figures 5F and S4A, H).

Discussion

Despite the high sequence identity between p63 and p73 both proteins are involved in rather different biological processes. ChIPseq analyses of p63 and p73 have revealed largely overlapping promoter binding sites suggesting that the difference in biological function between both proteins is less due to distinct transcriptional targets than due to different tissue specific expression patterns (Yang et al., 2010). In addition, differences in the regulatory mechanisms of both proteins have been noticed before and likely contribute to their divergent biological functions. In contrast to p73, which is a constitutive tetramer in all expressed isoforms, the activity of the longest p63 isoform, TAp63α, is regulated through its

oligomeric state. In the current study, we show that the decisive difference between p63 on the one hand and p73 as well as p53 on the other hand is the organization of the N-terminal TA. In p63 this TA consists of a single domain that combines sequence elements of both the p53 TA1 and TA2 subdomains. The p73 transactivation domain is also divided into two separate domains of which, however, only TA1 binds strongly to the Taz2 domain of p300, while for the TA2 domain we could not identify the binding site in our NMR experiments. In contrast to all other Taz2-peptide structures the unmodified p73 TA1 adopts a different position and orientation due to its low aliphacity within the classical Mdm2 binding motif and the presence of two aromatic residues C-terminal to the classical TA1 peptide. The low binding affinity of the TA2 domain manifested by the absence of long range NOEs in our NMR experiments is consistent with an earlier study that using fluorescence anisotropy measurements demonstrated that TA1 is the main contributor to binding affinity (Burge et al., 2009). In contrast, in case of the p53 – Taz2 interaction, TA2 provides the largest share of binding energy (Krois et al., 2016).

Of all three family members, the interaction of p73 with the Taz2 domain is the weakest but can be enhanced by phosphorylation. Phosphorylation of T14 has been shown to significantly enhance the interaction with the Taz2 domain and a T14D phosphomimetic mutation showed a higher transactivation potential in cell culture studies (Burge et al., 2009). This phosphorylation also increased the affinity to the Taz1, Kix and NCBD domains, however, starting from very weak interactions in the non-modified forms. In addition, a similar phosphorylation study of the p53 TA domain has shown that multiple phosphorylation events enhance the affinity in an approximately linear manner. This observation led to the model of a rheostat that allows p53 to respond gradually and not switch like to increasing levels of cellular stress (Lee et al., 2010).

In the case of p63 the unmodified transactivation domain already shows high affinity to the p300 Taz2 domain. The main regulatory mechanism is the formation of the closed dimeric state. Our experiments suggest that the total inhibitory mechanism consists of two parts: 1) inhibition of the DNA binding activity and 2) inhibition of binding to the transcriptional machinery. A quantitative analysis of the inhibitory effect is, unfortunately, difficult and would require interaction studies of p300 fragments containing all four domains (Taz1, Taz2, NCBD, Kix) that can interact with the transactivation domains with both an open tetramer and the closed dimer. High expression levels always create some open conformation as well, further complicating *in vitro* binding studies (Kehrloesser et al., 2016). However, based on the pulldown and the fluorescence anisotropy studies we estimate that binding of a single TA domain to Taz2 is inhibited at least fiftyfold (observed affinity for the TA – Taz2 interaction: K_D= 200 nM, estimated affinity for the closed dimer – Taz2 interaction: K_D > 10µM). This is a conservative estimation based on the assumption that affinities lower than 10 µM would not

be visible in pulldown assays. Combined with the twentyfold inhibition of the DNA binding affinity, this creates a total inhibition efficiency of at least a factor 1000.

Our domain swap experiments have also revealed that TAp73α can be converted into a closed dimer. This transformation requires the sequences harboring the two hydrophobic motifs ILF and IIM of p63. These two motifs form one β-strand each that together with the β-strand from the C-terminal TI domain are part of a six-stranded anti-parallel β-sheet that inhibits the tetramerization interface (Coutandin et al., 2016). In previous experiments, we had shown that this N-terminal region of TAp63α is the kinetically most labile one. Introducing proteolytic cleavage sites either C-terminally to the TA domain (between residues 66 and 67) or N-terminally to the TI domain (between residues 591 and 592) revealed that cleavage after the TA domain results in a fast conversion of the closed dimeric state into an open tetrameric conformation, while TAp63α cleaved at the C-terminus remained in the closed dimeric state (Coutandin et al., 2016). Our previous results combined with the current data suggest that during evolution changes in the N-terminal region were sufficient to make all p73 isoforms constitutive open tetramers. At the same time the regions harboring the two hydrophobic patches that are necessary to keep TAp63α in the closed dimeric state evolved into a second transactivation domain that in p53 finally became the dominant one, whereas the TA1 domain plays a major role in regulation of p53's activity via binding to Mdm2.

Acknowledgements

The research was funded by the DFG (DO 545/8 and DO 545/13), the Centre for Biomolecular Magnetic Resonance (BMRZ), and the Cluster of Excellence Frankfurt (Macromolecular Complexes). M.T. was supported by a fellowship from the Fonds of the Chemical Industry.

Author contributions

Conceptualization, K.K., J.G., V.D. and S.K.; Methodology, K.K., J.G., Si.K., F.L., V.D. and S.K.; Investigation, K.K., J.G., Si.K., M.T., B.S. and F.L., Funding Acquisition, P.G. and V.D.; Resources, J.K.; Writing, K.K., J.G., V.D. and S.K.

Declaration of interests

The authors declare no competing interests.

References

BOLCUN-FILAS, E., RINALDI, V. D., WHITE, M. E. & SCHIMENTI, J. C. 2014. Reversal of female infertility by Chk2 ablation reveals the oocyte DNA damage checkpoint pathway. *Science,* 343**,** 533-6.

BURGE, S., TEUFEL, D. P., TOWNSLEY, F. M., FREUND, S. M., BYCROFT, M. & FERSHT, A. R. 2009. Molecular basis of the interactions between the p73 N terminus and p300: effects on transactivation and modulation by phosphorylation. *Proc Natl Acad Sci U S A,* 106**,** 3142-7.

COUTANDIN, D., OSTERBURG, C., SRIVASTAV, R. K., SUMYK, M., KEHRLOESSER, S., GEBEL, J., TUPPI, M., HANNEWALD, J., SCHAFER, B., SALAH, E., MATHEA, S., MULLER-KULLER, U., DOUTCH, J., GREZ, M., KNAPP, S. & DOTSCH, V. 2016. Quality control in oocytes by p63 is based on a spring-loaded activation mechanism on the molecular and cellular level. *Elife,* 5, e13909.

DERRY, W. B., PUTZKE, A. P. & ROTHMAN, J. H. 2001. Caenorhabditis elegans p53: role in apoptosis, meiosis, and stress resistance. *Science,* 294**,** 591-5.

DEUTSCH, G. B., ZIELONKA, E. M., COUTANDIN, D., WEBER, T. A., SCHAFER, B., HANNEWALD, J., LUH, L. M., DURST, F. G., IBRAHIM, M., HOFFMANN, J., NIESEN, F. H., SENTURK, A., KUNKEL, H., BRUTSCHY, B., SCHLEIFF, E., KNAPP, S., ACKER-PALMER, A., GREZ, M., MCKEON, F. & DOTSCH, V. 2011. DNA Damage in Oocytes Induces a Switch of the Quality Control Factor TAp63alpha from Dimer to Tetramer. *Cell,* 144**,** 566-76.

FENG, H., JENKINS, L. M., DURELL, S. R., HAYASHI, R., MAZUR, S. J., CHERRY, S., TROPEA, J. E., MILLER, M., WLODAWER, A., APPELLA, E. & BAI, Y. 2009. Structural basis for p300 Taz2-p53 TAD1 binding and modulation by phosphorylation. *Structure,* 17**,** 202-10.

GEBEL, J., TUPPI, M., KRAUSKOPF, K., COUTANDIN, D., PITZIUS, S., KEHRLOESSER, S., OSTERBURG, C. & DOTSCH, V. 2017. Control mechanisms in germ cells mediated by p53 family proteins. *J Cell Sci*, 130, 2663–2671.

GUNTERT, P. & BUCHNER, L. 2015. Combined automated NOE assignment and structure calculation with CYANA. *J Biomol NMR,* 62**,** 453-71.

GUNTERT, P., MUMENTHALER, C. & WUTHRICH, K. 1997. Torsion angle dynamics for NMR structure calculation with the new program DYANA. *J Mol Biol,* 273**,** 283-98.

KEHRLOESSER, S., OSTERBURG, C., TUPPI, M., SCHAFER, B., VOUSDEN, K. H. & DOTSCH, V. 2016. Intrinsic aggregation propensity of the p63 and p73 TI domains correlates with p53R175H interaction and suggests further significance of aggregation events in the p53 family. *Cell Death Differ*, 23, 1952-1960.

KORADI, R., BILLETER, M. & GUNTERT, P. 2000. Point-centered domain decomposition for parallel molecular dynamics simulation. *Computer Physics Communications,* 124**,** 139-147.

KROIS, A. S., FERREON, J. C., MARTINEZ-YAMOUT, M. A., DYSON, H. J. & WRIGHT, P. E. 2016. Recognition of the disordered p53 transactivation domain by the transcriptional adapter zinc finger domains of CREB-binding protein. *Proc Natl Acad Sci U S A,* 113**,** E1853-62.

KUSSIE, P. H., GORINA, S., MARECHAL, V., ELENBAAS, B., MOREAU, J., LEVINE, A. J. & PAVLETICH, N. P. 1996. Structure of the MDM2 oncoprotein bound to the p53 tumor suppressor transactivation domain. *Science,* 274**,** 948-53.

LEE, C. W., FERREON, J. C., FERREON, A. C., ARAI, M. & WRIGHT, P. E. 2010. Graded enhancement of p53 binding to CREB-binding protein (CBP) by multisite phosphorylation. *Proc Natl Acad Sci U S A,* 107**,** 19290-5.

LOHR, F., HANSEL, R., ROGOV, V. V. & DOTSCH, V. 2007. Improved pulse sequences for sequence specific assignment of aromatic proton resonances in proteins. *J Biomol NMR,* 37**,** 205-24.

LOVELL, S. C., WORD, J. M., RICHARDSON, J. S. & RICHARDSON, D. C. 2000. The penultimate rotamer library. *Proteins,* 40**,** 389-408.

LUH, L. M., KEHRLOESSER, S., DEUTSCH, G. B., GEBEL, J., COUTANDIN, D., SCHAFER, B., AGOSTINI, M., MELINO, G. & DOTSCH, V. 2013. Analysis of the oligomeric state and transactivation potential of TAp73alpha. *Cell Death Differ,* 20**,** 1008-16.

MILLER JENKINS, L. M., FENG, H., DURELL, S. R., TAGAD, H. D., MAZUR, S. J., TROPEA, J. E., BAI, Y. & APPELLA, E. 2015. Characterization of the p300 Taz2-p53 TAD2 complex and comparison with the p300 Taz2-p53 TAD1 complex. *Biochemistry,* 54**,** 2001-10.

MILLS, A. A., ZHENG, B., WANG, X. J., VOGEL, H., ROOP, D. R. & BRADLEY, A. 1999. p63 is a p53 homologue required for limb and epidermal morphogenesis. *Nature,* 398**,** 708-13.

OLLMANN, M., YOUNG, L. M., DI COMO, C. J., KARIM, F., BELVIN, M., ROBERTSON, S., WHITTAKER, K., DEMSKY, M., FISHER, W. W., BUCHMAN, A., DUYK, G., FRIEDMAN, L., PRIVES, C. & KOPCZYNSKI, C. 2000. Drosophila p53 is a structural and functional homolog of the tumor suppressor p53. *Cell,* 101**,** 91-101.

PETERS, M. B., YANG, Y., WANG, B., FUSTI-MOLNAR, L., WEAVER, M. N. & MERZ, K. M., JR. 2010. Structural Survey of Zinc Containing Proteins and the Development of the Zinc AMBER Force Field (ZAFF). *J Chem Theory Comput,* 6**,** 2935-2947.

PONDER, J. W. & CASE, D. A. 2003. Force fields for protein simulations. *Protein Simulations,* 66**,** 27-85.

PREHODA, K. E., SCOTT, J. A., MULLINS, R. D. & LIM, W. A. 2000. Integration of multiple signals through cooperative regulation of the N-WASP-Arp2/3 complex. *Science,* 290**,** 801-6.

SERBER, Z., LAI, H. C., YANG, A., OU, H. D., SIGAL, M. S., KELLY, A. E., DARIMONT, B. D., DUIJF, P. H., VAN BOKHOVEN, H., MCKEON, F. & DOTSCH, V. 2002. A C-terminal inhibitory domain controls the activity of p63 by an intramolecular mechanism. *Mol Cell Biol,* 22**,** 8601-11.

SHEN, Y., DELAGLIO, F., CORNILESCU, G. & BAX, A. 2009. TALOS+: a hybrid method for predicting protein backbone torsion angles from NMR chemical shifts. *J Biomol NMR,* 44**,** 213-23.

STRAUB, W. E., WEBER, T. A., SCHAFER, B., CANDI, E., DURST, F., OU, H. D., RAJALINGAM, K., MELINO, G. & DOTSCH, V. 2010. The C-terminus of p63 contains multiple regulatory elements with different functions. *Cell Death & Disease,* 1**,** e5.

SUH, E. K., YANG, A., KETTENBACH, A., BAMBERGER, C., MICHAELIS, A. H., ZHU, Z., ELVIN, J. A., BRONSON, R. T., CRUM, C. P. & MCKEON, F. 2006. p63 protects the female germ line during meiotic arrest. *Nature,* 444**,** 624-8.

TUPPI, M., KEHRLOESSER, S., COUTANDIN, D. W., ROSSI, V., LUH, L. M., STRUBEL, A., HOTTE, K., HOFFMEISTER, M., SCHAFER, B., DE OLIVEIRA, T., GRETEN, F., STELZER, E. H. K., KNAPP, S., DE FELICI, M., BEHRENDS, C., KLINGER, F. G. & DOTSCH, V. 2018. Oocyte DNA damage quality control requires consecutive interplay of CHK2 and CK1 to activate p63. *Nat Struct Mol Biol*, 25, 261-269.

VAN DEN ENT, F. & LOWE, J. 2006. RF cloning: a restriction-free method for inserting target genes into plasmids. *J Biochem Biophys Methods,* 67**,** 67-74.

WOODARD, T. L. & BOLCUN-FILAS, E. 2016. Prolonging Reproductive Life after Cancer: The Need for Fertoprotective Therapies. *Trends Cancer,* 2**,** 222-233.

YAMAZAKI, T., FORMANKAY, J. D. & KAY, L. E. 1993. 2-Dimensional Nmr Experiments for Correlating C-13-Beta and H-1-Delta/Epsilon Chemical-Shifts of Aromatic Residues in C-13-Labeled Proteins Via Scalar Couplings. *Journal of the American Chemical Society,* 115**,** 11054-11055.

YANG, A., KAGHAD, M., WANG, Y., GILLETT, E., FLEMING, M. D., DOTSCH, V., ANDREWS, N. C., CAPUT, D. & MCKEON, F. 1998. p63, a p53 homolog at 3q27-29, encodes multiple products with transactivating, death-inducing, and dominant-negative activities. *Mol Cell,* 2**,** 305-16.

YANG, A., SCHWEITZER, R., SUN, D., KAGHAD, M., WALKER, N., BRONSON, R. T., TABIN, C., SHARPE, A., CAPUT, D., CRUM, C. & MCKEON, F. 1999. p63 is essential for regenerative proliferation in limb, craniofacial and epithelial development. *Nature,* 398**,** 714-8.

YANG, A., ZHU, Z., KETTENBACH, A., KAPRANOV, P., MCKEON, F., GINGERAS, T. R. & STRUHL, K. 2010. Genome-wide mapping indicates that p73 and p63 co-occupy target sites and have similar dna-binding profiles in vivo. *PLoS One,* 5**,** e11572.

YU, B., MARTINS, I. R., LI, P., AMARASINGHE, G. K., UMETANI, J., FERNANDEZ-ZAPICO, M. E., BILLADEAU, D. D., MACHIUS, M., TOMCHICK, D. R. & ROSEN, M. K. 2010. Structural and energetic mechanisms of cooperative autoinhibition and activation of Vav1. *Cell,* 140**,** 246-56.

Figure titles and legends

Figure 1. The interaction of p63 with p300 domains is isoform dependent

The ability of the p300 domains Taz1 and Taz2 to bind different p63 and p73 isoforms was determined via pull-down assay. Data is presented as mean ± SD (*n* = 3). IN: input, represents 1% of total expression. PD: pull-down. The shown western blot for GST-Taz2 pull down experiments is split into two different experiments as the expression level for TAp63α was generally very low and required different exposure times.

Figure 2. Exon 1 and exon 2 confer to high transcriptional potential of TAp63

(A) Wildtype domain structure of TAp73α, -β, TAp63α and TAp63γ that have been used as references throughout the experiments and overview of chimeric constructs that are based on TAp73α, TAp73β and TAp63α. Using a restriction free cloning technique major domains and regions were exchanged between p63 and p73 in order to map the oligomeric state and transactivation capability of single domains and distinct regions (TAp73α/ β_p63 aa2-69, _p63DBD: p73aa 126-311>p63aa 137-322, _p63TD: p73aa 308-394>p63AA319-406, TAp63α_p73TA: p63AA2-107>p73aa 2-96, _p73TD: p63aa 319-406>p73aa308-394, _p73CTD: p63aa 570-641>p73aa 553-636). TA: transactivation domain, DBD: DNA binding domain, TD: tetramerization domain, SAM: sterile alpha motif, TI: transactivation inhibitory domain, CTD: C-terminal domain.

(B) Transactivation potential of TAp73β, TAp63γ and different p73/p63 chimera measured in Saos2 cells on the p21-promoter. Fold induction was normalized to the positive control TAp63γ.

(C) Transactivation assays with p73 chimeras containing either exon1 (p63 amino acids 2-25) or exon1+2 (p63 amino acids 2-69) of p63. The transactivation level was compared to TAp73β and TAp63γ. Data is presented as mean ± SD (*n* = 3).

See also Figure S1.

Figure 3. TAp63 contains only one transactivation domain

(A) The transactivation potential of p53, TAp63γ and TAp73β containing alanine mutations of the FWL, IIM or ILF motif was determined. Fold induction was normalized to TAp63γ. Data presented as mean ± SD (*n* = 3).

(B) Sequence alignment of the p53 TA2 and the p63 TA domains. Color intensities correspond to the degree of homology.

(C) The region responsible for high transactivation potential in p63 was further defined by measuring the transactivation potential TAp73β chimeras harboring amino acids 2-15, 16-25 or 8-15 of p63. Fold induction was normalized to TAp63γ. Data is presented as mean ± SD (*n* = 3).

(D) Fluorescence anisotropy curves for TA peptides of p63, p73 and a hybrid between both TA domains. Calculated dissociation constants are given. Measurements were carried out at room temperature (20 °C) and repeated at least in duplicates. Data is presented as mean ± SD between measurements (*n* = 2).

See also Figure S1.

Figure 4. Structures of p300 Taz2 fused to the TA domains of p63, p73 and p53

(A) Overlay of the structures of the p63 TA with the TA2 of p53 (PDB: 5HP0) upon binding to p300 or CBP Taz2.

(B), (D), (F) show the fusion constructs of p300Taz2-p63TA, p300Taz2-p73TA1 or CBPTaz2-p53AD2 (PDB: 5HP0) as ribbon diagrams, respectively. All constructs are depicted in a similar orientation. Taz2 is shown in blue, the corresponding peptide in orange, the linker in green and zinc ions in yellow.

(C), (E), (G) show the same structures as before, but with the Taz2 domain as space filling model. The TA peptides are shown in rainbow colors from N (blue) to C (red) terminus. The surfaces of the Taz2 domains are shown in grey with hydrophobic amino acids depicted in pale cyan. Major interacting amino acids are shown as sticks.

See also Table 1, Table 2 and Figures S2, S3.

Figure 5. Exon 2 of p63 confers ability to form a dimeric conformation to p73

(A), (B) SEC analysis of TAp73α compared to chimeras harboring (A) either exon1 and exon 2 of p63 (amino acids 2-69) or (B) only exon1 (amino acids 2-25) expressed in rabbit reticulocyte lysate.

(C), (D) SEC analysis of TAp63α compared to chimeras harboring (C) either amino acids 2-25 or (D) the C-terminal domain (amino acids 553-636) of p73.

(E), (F) SEC analysis of TAp63α compared to chimeras harboring (E) the TD or (F) the TA domain (amino acids 2-96) of p73. SEC analysis was performed with a Superose 6 PC3.2/30 column. Calibration of the Superose 6 column was used as described previously (Deutsch et al., 2011). See also Figure S4.

Table 1: Structure calculation statistics p300Taz2-p63TA.

Automated NOE assignment (a)	**CYANA result**	**energy minimized** (b)
^{15}N-resolved NOESY cross peaks	1283	
^{13}C-resolved NOESY cross peaks	2227	
^{13}C-resolved aromatic NOESY cross peaks	428	
Total number of NOESY cross peaks	3938 (100%)	
Assigned cross peaks (d)	3019 (76.7%)	
Unassigned cross peaks (d)	919 (23.3%)	
Structural restraints		
Assigned NOE distance restraints (e)	1565 (100%)	
Short range |i-j|≤1	899 (57.4%)	
Medium range 1<|i-j|<5	385 (24.6%)	
Long range |i-j|≥5	281 (18.0%)	
Dihedral angle restraints (φ/ψ)	182	
Restraints for zinc coordination (upl/lol)	48	
Structure statistics		
Average CYANA target function value (Å^2)	1.90 ± 0.16	1.88 ± 0.38
Average AMBER Energies (kcal/mol)	-3859.73 ± 133.03	-4818.54 ± 109.39
Restraint violations (c)		
Max. distance restraint violation (Å)	0.50	0.12
Number of violated distance restraints > 0.2 Å	0	0
Max. dihedral angle restraint violations (°)	5.96	4.71
Number of violated dihedral angle constraints > 5°	0	0
Ramachandran plot		
Residues in most favored regions	80.5%	84.3%
Residues in additionally allowed regions	19.5%	15.2%
Residues in generously allowed regions	0.0%	0.5%
Residues in disallowed regions	0.0%	0.0%
RMSD (residues 7..48, 59..91, 101..114		
Average backbone RMSD to mean (Å)	0.52 ± 0.06	0.58 ± 0.07
Average heavy atom RMSD to mean (Å)	0.96 ± 0.08	1.02 ± 0.09

(a) using structure calculation functionalities of CYANA

(b) after restrained energy minimization with OPALp

(c) after energy minimization, calculated with CYANA

(d) in parenthesis the percentage of the total cross peaks

(e) in parenthesis the percentage of the total distance restraints from the peak assignment

Table 2: Structure calculation statistics p300Taz2-p73TA1.

Automated NOE assignment (a)	**CYANA result**	**energy minimized** (b)
^{15}N-resolved NOESY cross peaks	1278	
^{13}C-resolved NOESY cross peaks	2719	
^{13}C-resolved aromatic NOESY cross peaks	409	
^{13}C-^{13}C-resolved NOESY (4D)	159	
Total number of NOESY cross peaks	4565 (100%)	
Assigned cross peaks (d)	3031 (66.4%)	
Unassigned cross peaks (d)	1534 (33.6%)	
Structural restraints		
Assigned NOE distance restraints (e)	1563 (100%)	
Short range $\|i-j\|\leq 1$	881 (56.4%)	
Medium range $1<\|i-j\|<5$	387 (24.8%)	
Long range $\|i-j\|\geq 5$	295 (18.9%)	
Dihedral angle restraints (φ/ψ)	174	
Restraints for helix definition (upl/lol; residues 8..24)	32	
Restraints for zinc coordination (upl/lol)	46	
Structure statistics		
Average CYANA target function value (Å^2)	1.45 ± 0.16	2.36 ± 0.45
Average AMBER Energies (kcal/mol)	-3933.45 ± 99.80	-4964.04 ± 92.86
Restraint violations (c)		
Max. distance restraint violation (Å)	0.28	0.15
Number of violated distance restraints > 0.2 Å	0	0
Max. dihedral angle restraint violations (°)	7.81	3.48
Number of violated dihedral angle constraints > 5°	0	0
Ramachandran plot		
Residues in most favored regions	81.9%	84.3%
Residues in additionally allowed regions	18.0%	15.1%
Residues in generously allowed regions	0.1%	0.5%
Residues in disallowed regions	0.0%	0.0%
RMSD (residues 7..91, 113..130)		
Average backbone RMSD to mean (Å)	0.67 ± 0.17	0.72 ± 0.16
Average heavy atom RMSD to mean (Å)	1.07 ± 0.15	1.14 ± 0.14

(a) using structure calculation functionalities (CYANA), (b) after restrained energy minimization (OPALp), (c) after energy minimization (CYANA), (d) in parenthesis the percentage of the total cross peaks, (e) in parenthesis the percentage of the total distance restraints from the peak assignment

CONTACT FOR REAGENT AND RESOURCE SHARING

Further information and requests for resources and reagents should be directed to and will be fulfilled by the Lead Contact, Volker Dötsch (vdoetsch@em.uni-frankfurt.de).

METHOD DETAILS

Restriction free cloning

Primers were designed with complementary sequence to the desired insert. The inserts were amplified, the resulting products were purified and used in a second PCR using the destination plasmids as templates. DpnI was used to degrade the parental plasmids and purify the hybrid plasmids (van den Ent and Lowe, 2006).

Pull-down experiments

Pull-downs were performed as described previously (Straub et al., 2010). Pull-down experiments were carried out in centrifugal filtration units using a Durapore membrane with a pore size of 0.65 µm (Millipore UFC30DV00) and a table top centrifuge operating at 1000 r.p.m. In general, 125 µg of GST-fused bait protein (bacterially expressed and purified) was incubated for 60 min with 50 µl of Glutathione resin pre-equilibrated in pull-down buffer (180 mM NaCl, 0.1% Tween-20, 50 mM Tris pH 8.0, 10 mM β-mercapto-ethanol). The resin was washed four times with 400 µl of pull-down buffer to remove excess GST-fused bait protein. Expression of target constructs was done in rabbit reticulocyte lysate, as described previously in a total volume of 50 µl (Promega) (Straub et al., 2010). A volume of 5 µl of the reaction mixture was removed for use as an input control, resulting after mixing with 45 µl of SDS loading buffer and running of 5 µl on an SDS PAGE in the 1% input signal. The remaining 45 µl were incubated with the GST–fusion bait protein resin for 2 h at room temperature and then centrifuged. The resin was washed 4 times with 400 µl of pull-down buffer and the bound proteins were eluted with 2x20 µl of 4x hot SDS-PAGE buffer. Analysis after SDS-PAGE was performed by western blotting.

Relative pull-down efficiencies were determined by dividing the quantified Western blot signals for pull-down and input. 90% of the expression was used for the assay and 25% of the subsequent elution for SDS PAGE analysis and western blotting. A normalization factor was introduced to correct for the different fractions of input and pull-down, which have been loaded onto the gel, in relation to the volume of protein expression. Quantification and normalization were performed separately for each pull-down. Experiments were repeated at least in triplicates.

Cell culture and transactivation assay

The human neuroblastoma cell line SK-N-AS and the osteosarcoma cell line Saos2 were cultured in DMEM (with glutamine) containing 10% FBS (Capricorn Scientific) and 100 µg/ml Penicillin/Streptomycin. For SK-N-AS cells growth medium was further supplemented with 1 mM sodium pyruvate. SK-N-AS and Saos2 cells were transfected with 100 ng per plasmid (pcDNA, pGL3 and pcRMV) using Qiagen Effectene according to manufacturer's recommendation in a 12-well plate and grown for 20-24 h. Transactivation experiments were performed using the Promega Dual-Glo Luciferase reporter assay. Cells were harvested and subsequently assayed for Firefly and Renilla activity in a 96-well plate four times. After determining the Firefly to Renilla ratio, Grubb's test was used to calculate outliers. Three independent experiments have been performed for each transactivation assay. The rest of the sample was used for determining expression levels via Western blot.

Western blot:

Western blotting was performed as described previously (Deutsch et al., 2011) loading 25% of cell lysate. The following antibodies were used: anti-myc (clone 4A6, Millipore) and anti-GAPDH (clone 6C5, Millipore). Western blot signals were quantified using ImageJ.

Size exclusion chromatography:

Size exclusion chromatography experiments with proteins expressed in rabbit reticulocyte lysate transcription/ translation system (Promega) were performed as previously described (Deutsch et al., 2011) at 4°C using a Superose 6 PC 3.2/300 column (GE Healthcare) with an injection volume of 50µL.

Protein expression:

Taz2

A codon optimized version of p300 Taz2 (residues 1723-1812) was subcloned into a pMAL-c4x vector including a TEV cleavage site between MBP and Taz2. All cysteines, which do not participate in zinc coordination, were mutated to alanines (C1738, C1746, C1769, C1770). Protein expression was performed in T7 express cells (NEB) in 2xYT medium supplemented with 100 µM $ZnCl_2$ for 16 h at 22°C. Labeled protein expression was performed in M9 medium with addition of 1 g/l of $^{15}NH_4Cl$ and 2 g/l ^{13}C glucose.

Cells were harvested by centrifugation and resuspended in cold lysis buffer (25 mM Tris, 1000 mM NaCl, 20 mM beta-mercaptoethanol pH 7.8) under the addition of protease inhibitor and DNAse. After sonication and subsequent cell debris removal by high speed

centrifugation the cell lysate was loaded onto a MBP column. Protein was eluted with elution buffer (25 mM Tris, 500 mM NaCl, 20 mM Maltose, 20 mM beta-mercaptoethanol, pH 7.8). TEV cleavage was performed overnight at room temperature. To remove MBP and MBP-TEV protease a zinc-affinity chromatography was performed. The protein was loaded, and shortly washed with buffer (25 mM Tris, 500 mM NaCl, 10 mM beta-mercaptoethanol, pH 7.8) and eluted with elution buffer (25 mM Tris, 500 mM NaCl, 500 mM imidazole, 10 mM beta-mercaptoethanol, pH 7.8). Protein containing fractions were pooled and supplemented with $ZnCl_2$ to 10 mM, TCEP to 1 mM and protease inhibitor. This mixture was left standing overnight at 4 °C. The next day the protein was concentrated (Amicon Centrifugal Filter 10 kDa MWCO) and subject to gel filtration either into NMR buffer or ITC buffer (both described below).

Protein used for the Peptide Spot Assay was expressed and purified as described above. However instead of TEV cleavage the MBP-Taz2 fusion protein was subject to anion exchange chromatography to remove fragmented protein. Eluted full length protein was concentrated and gel filtered into TBS buffer.

Taz2-p63TA/Taz2-p73TA1 fusion constructs

The Taz2 construct described above was c-terminally elongated by restriction free cloning with a short linker and the p63 TA or p73 TA1 respectively. Protein expression and purification of fusion constructs was performed as described above, up to the point of TEV cleavage. The fusion constructs were subject to cation exchange chromatography to remove MBP and MBP-TEV (Buffer A: 25 mM MOPS, 20 mM beta-mercaptoethanol, pH 7.0; Buffer B: 25 mM MOPS, 1000 mM NaCl, 20 mM beta-mercaptoethanol, pH 7.0). The protein was eluted with a linear salt gradient to 100% buffer B. All protein containing fractions were pooled, concentrated and subject to gel filtration into NMR buffer (25 mM MES, 200 mM NaCl (p63) or 50 mM NaCl (p73), 0.5 mM TCEP, pH 6.3).

Fluorescence anisotropy

Peptides were either ordered from N-terminally Fluorescein-tagged from Genscript (Piscataway, USA) or N-terminally cysteine-tagged from Peps4LS (Heidelberg, Germany). Cysteine tagged peptides were labeled with a 10-fold molar excess of 5-(Iodoacetamido)fluorescein for 1 h and subsequently the buffer was exchanged by using a Superdex 75 column (GE Healthcare, Chicago, USA) to remove additional dye. The mass of the labeled peptides was confirmed by MALDI-MS.

Fluorescence anisotropy was measured with a FP-6500 spectrometer (Jasco, Gross-Umstadt, Germany) at 22°C and a 108F-QS cuvette (Hellma, Müllheim, Germany). Peptide

concentration was constant at 100 nM for all samples and protein concentration was increased in a pseudo-exponential manner.

NMR spectroscopy

All u^{13}C/u^{15}N labeled proteins samples were measured in buffer containing 25 mM MES, 50 mM NaCl (Taz2-p73 constructs) or 200 mM NaCl (Taz2 and Taz2-p63 constructs), 0.5 mM TCEP, 5% D_2O and DSS as an internal shift reference. Protein concentration generally ranged from 700 µM (p300Taz2-p73TA1) to 1200 µM (p300Taz2-p63TA).

Spectra were measured at a sample temperature of 30°C on Bruker Avance spectrometers with proton Larmor frequencies ranging from 600 MHz to 950 MHz. The backbone assignment resulted from 3D [^{15}N,^{1}H]-BEST-TROSY type HNCACB and HN(CA)CO spectra. Aliphatic side chain resonances were assigned with the help of 3D [^{15}N,^{1}H]-TROSY-(H)C(C)(CO)NH-TOCSY and [^{15}N,^{1}H]-TROSY H(CC)(CO)NH-TOCSY spectra. For aromatic side chains (HB)CB(CDCD)HD (Yamazaki et al., 1993) and (H)CB(CG)CCH-TOCSY (Lohr et al., 2007) spectra were used. Distance restraints were obtained from 3D ^{15}N-resolved NOESY-BEST-TROSY (τ_m=70 ms), 3D ^{13}C-resolved NOESY-HSQC (τ_m=70 ms) and a 4D [^{13}Cmethyl,^{1}H]-SOFAST-HMQC-NOESY-[^{13}Carom,^{1}H]-HMQC (τ_m=70 ms; p300Taz2-p73TA1 only) spectra. The protonation state of histidine residues involved in zinc-coordination was established with the help of His-sidechain [^{15}N,^{1}H]-HMBC spectra.

Structure calculation

The automated peak assignment strategy of CYANA (Guntert et al., 1997, Guntert and Buchner, 2015) was employed to generate restraints and calculate the structure of p300Taz2 with the TA domains of p63 and p73. The statistical results of this peak assignment and structure calculation are listed in Table 1 and Table 2. Peak lists from three experiments, an ^{15}N-resolved NOESY and a ^{13}C-resolved NOESY for the aliphatic and aromatic residues, respectively, were used. In the Taz2p73TA1 case an additional peak list from a 4D [^{13}Cmethyl,^{1}H]-SOFAST-HMQC-NOESY-[^{13}Carom,^{1}H]-HMQC experiment was used. Structural calculation in each cycle resulted in the best 20 structures out of 200 calculated structures with respect to the CYANA target function, using the 20 structures from the final cycle for the bundle representation. In each calculation a random starting structure was minimized in 20,000 torsion angle dynamic steps and the remaining CYANA parameters were kept at their default values. In addition to the automatic peak assignment based distance restraints, additional dihedral angle restraints obtained from chemical shift analysis by Talos+ (Shen et al., 2009) were used. In the case of Taz2p73TA1 some additional restraints were needed. Helical hydrogen contacts were enforced by additional restraints for the first helical

region (residues 8 to 24) determined by Talos+. As there is no experimental data on the many glycines of the linker region (residues 91 to 111), these glycines tend to form bad backbone conformations. We restricted the backbone torsional angles of the glycines in the linker region to the high populated Ramachandran plot. For the structure calculation of Taz2p63TA and Taz2p73TA1 rotamer library restraints were used. The employed rotamer library was a backbone depended library described in Lovell, S. C., et al. 2000 (Lovell et al., 2000) (downloaded from the web page in 2013). Restraints for zinc coordination were used as described in the following. Zinc tetrahedral coordination was enforced by constructing an additional CYANA library residue entry. In the residue entry the zinc atom is surrounded by four dummy atoms (atoms with no mass and no interaction with other atoms) rigidly connected to it, which are placed on the vertexes of a regular tetrahedron with the zinc atom as its center and edge length of 1 Å. In this manner, it is possible to enforce a tetrahedral coordination of each zinc by eight lower and upper distance restraints. The atom VdW radii of the zinc and the interacting nitrogen and sulfur atoms in the coordinating histidine and cysteine residues, respectively, were set to the radii defined by the Zinc AMBER force field (ZAFF) (Peters et al., 2010). The structural bundle was energy refined using OPALp (Koradi et al., 2000), which relies on the AMBER 94 force field (Ponder and Case, 2003), while the distance angular restraints from the structure calculation were included.

Structures were deposited in the PDB with accession codes 6FGN for the Taz2-p63 complex and 6FGS for the Taz2-p73 complex.

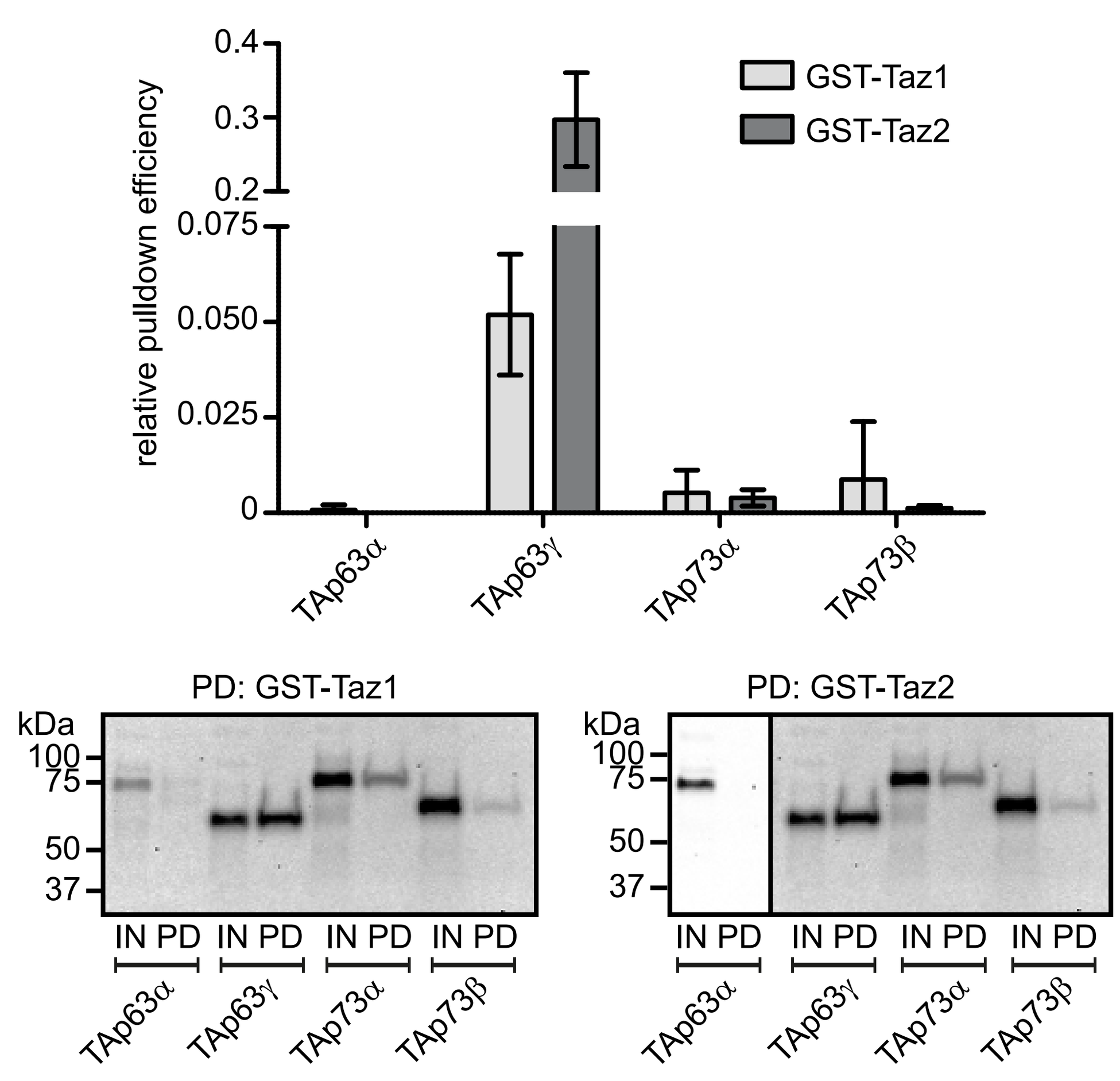
relative pulldown efficiency
0.4
0.3
0.2
0.075
0.050
0.025
0
GST-Taz1
GST-Taz2
TAp63α
TAp63γ
TAp73α
TAp73β
PD: GST-Taz1
PD: GST-Taz2
kDa
100
75
50
37
IN PD
IN PD
IN PD
IN PD
TAp63α
TAp63γ
TAp73α
TAp73β

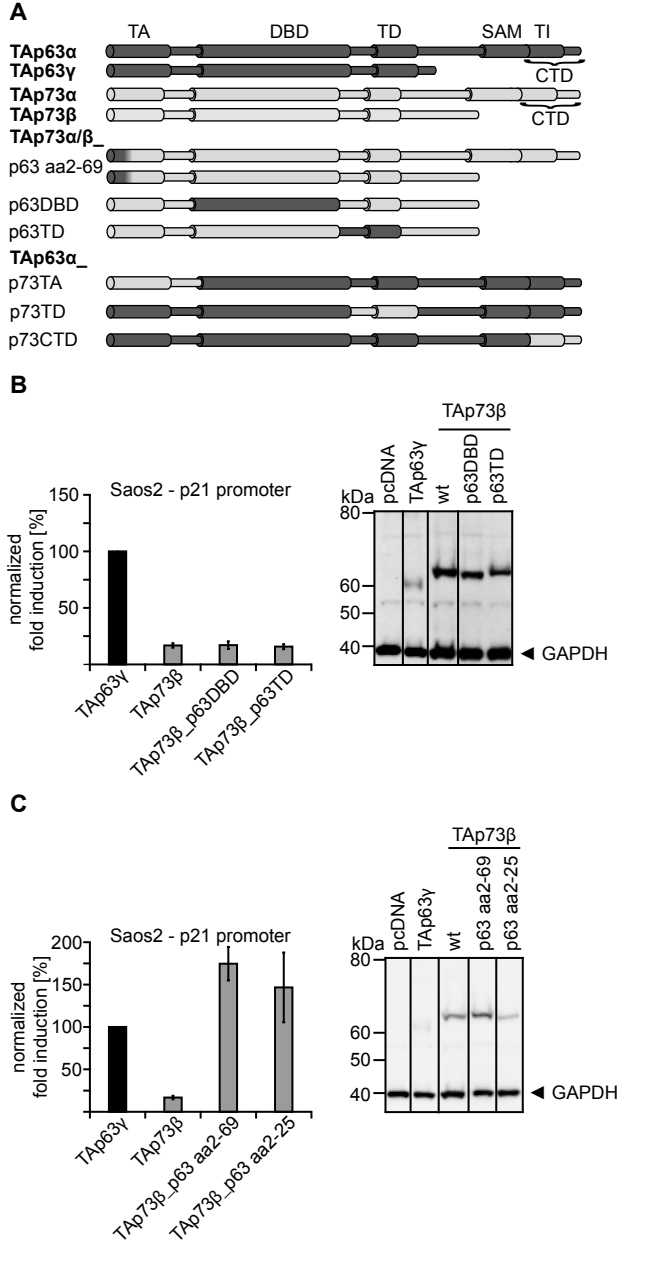
A
TA
DBD
TD
SAM
TI
TAp63α
TAp63γ
CTD
TAp73α
TAp73β
CTD
TAp73α/β_
p63 aa2-69
p63DBD
p63TD
TAp63α_
p73TA
p73TD
p73CTD
B
Saos2 - p21 promoter
normalized fold induction [%]
150
100
50
TAp63γ
TAp73β
TAp73β_p63DBD
TAp73β_p63TD
TAp73β
pcDNA
TAp63γ
wt
p63DBD
p63TD
kDa
80
60
50
40
GAPDH
C
Saos2 - p21 promoter
normalized fold induction [%]
200
150
100
50
TAp63γ
TAp73β
TAp73β_p63 aa2-69
TAp73β_p63 aa2-25
TAp73β
pcDNA
TAp63γ
wt
p63 aa2-69
p63 aa2-25
kDa
80
60
50
40
GAPDH

A

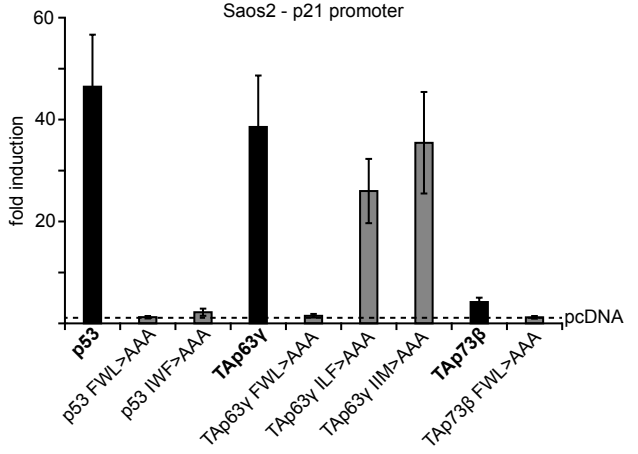

B

C

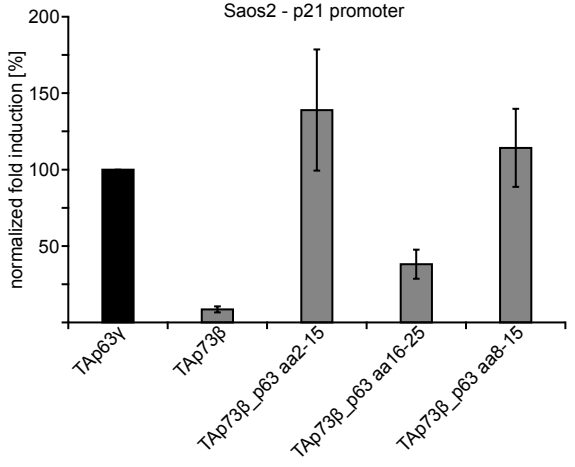

D

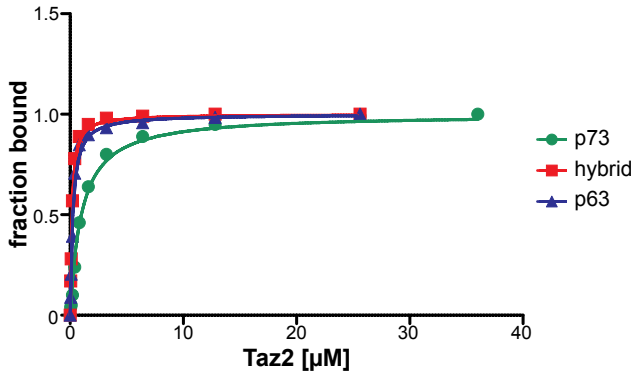

Peptide	Dissociation constant [μM]
p63 8-32	0.196±0.022
p73 8-31	0.944±0.064
p63 8-15/p73 15-31 hybrid	0.116±0.010

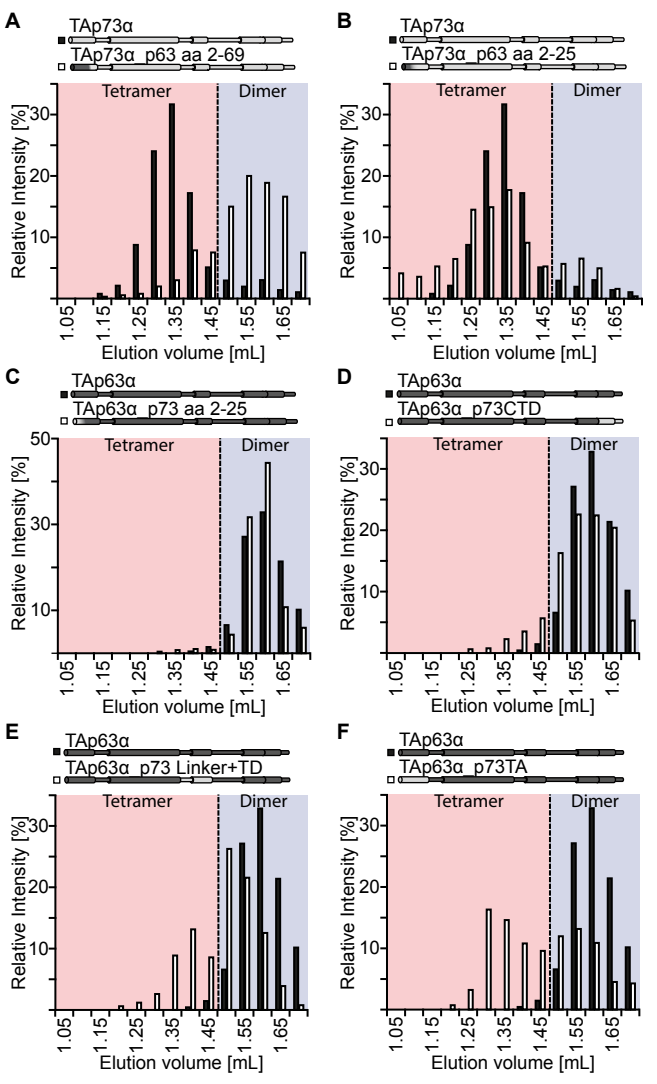
A
TAp73α
TAp73α p63 aa 2-69
Tetramer
Dimer
Relative Intensity [%]
Elution volume [mL]
B
TAp73α
TAp73α p63 aa 2-25
Tetramer
Dimer
Relative Intensity [%]
Elution volume [mL]
C
TAp63α
TAp63α p73 aa 2-25
Tetramer
Dimer
Relative Intensity [%]
Elution volume [mL]
D
TAp63α
TAp63α p73CTD
Tetramer
Dimer
Relative Intensity [%]
Elution volume [mL]
E
TAp63α
TAp63α p73 Linker+TD
Tetramer
Dimer
Relative Intensity [%]
Elution volume [mL]
F
TAp63α
TAp63α p73TA
Tetramer
Dimer
Relative Intensity [%]
Elution volume [mL]

Supplemental Material

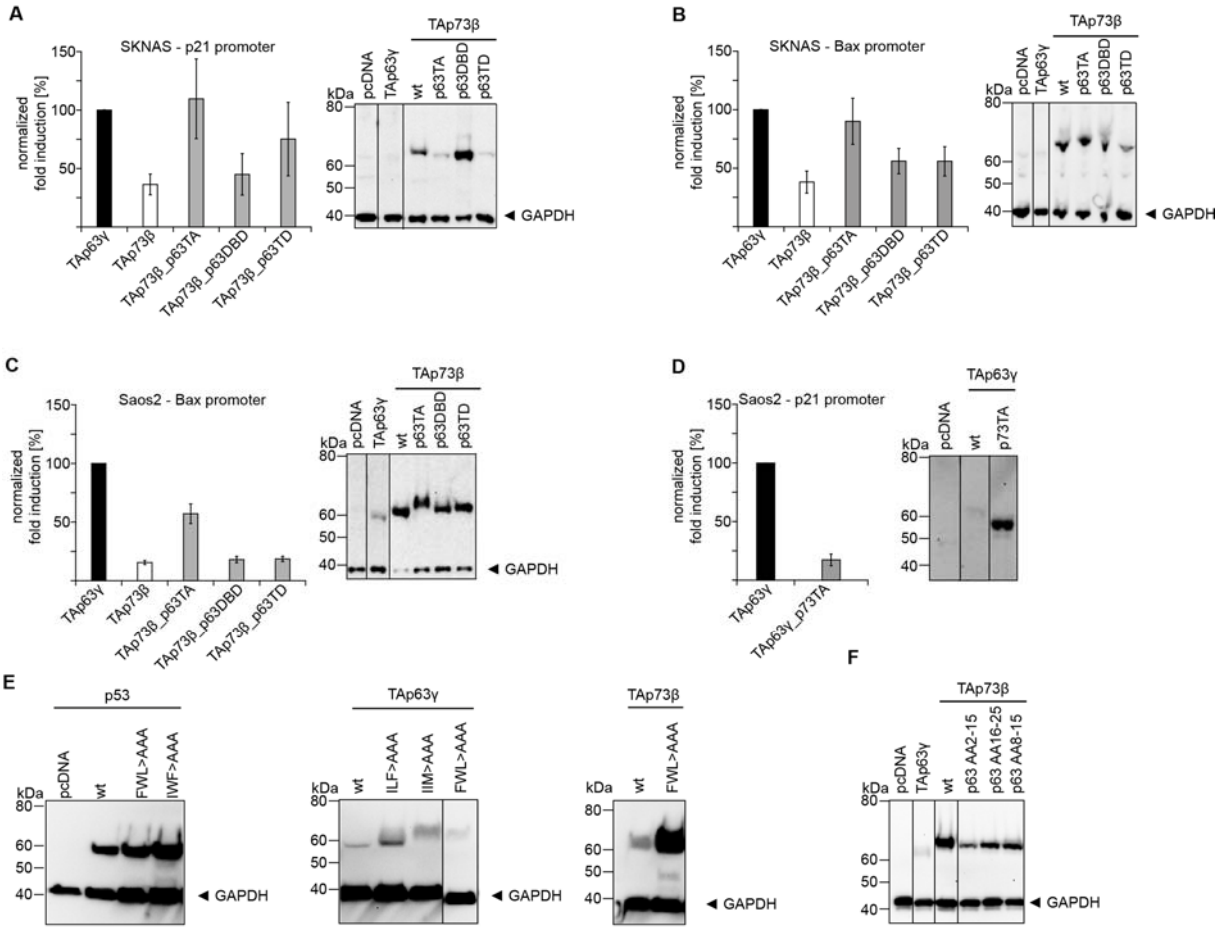

Figure S1. Related to Figure 2 and Figure 3.

The transactivation potential of TAp73β and chimeras harboring the complete p63 TA, DBD or TD, respectively, was measured in (A) SKNAS cells on the p21-promoter and (B) Bax-promoter as well as in (C) Saos2 cells on the Bax-promoter. (D) The transactivation potential of TAp63γ and chimeras containing the complete p73 TA, DBD or TD, respectively, was measured on the p21-promoter in Saos2 cells. Fold induction over empty vector was normalized to the positive control TAp63γ for all transactivation assays and transcription factor expression levels were monitored by Western blot. GAPDH was detected as a loading control in all Western blots. All transactivation assays were performed in triplicates. Each single data point was measured as four technical replicates, outliers have been identified using Grubb's test and corrected data have been averaged. Error bars represent the standard deviation. (E) and (F) represent the Western blots corresponding to the transactivation assays shown in Figure 3A and 3C. In all cases the western blots are from single experiments,

however in some cases lanes have been swapped so that in each blot the order of the blot matches to bar diagram.

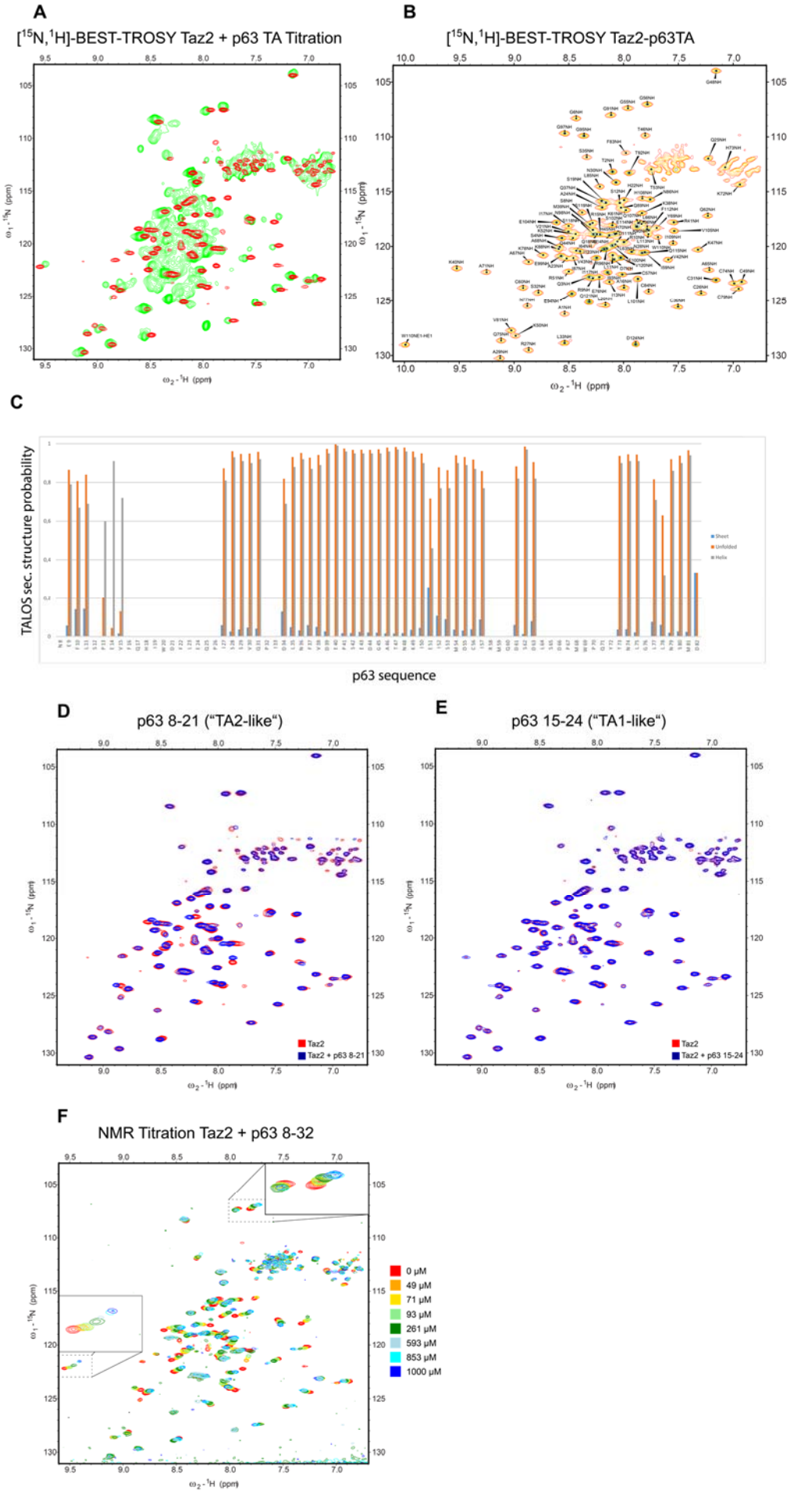
A
[15N,1H]-BEST-TROSY Taz2 + p63 TA Titration
B
[15N,1H]-BEST-TROSY Taz2-p63TA
C
TALOS sec. structure probability
p63 sequence
D
p63 8-21 ("TA2-like")
Taz2
Taz2 + p63 8-21
E
p63 15-24 ("TA1-like")
Taz2
Taz2 + p63 15-24
F
NMR Titration Taz2 + p63 8-32
0 µM
49 µM
71 µM
93 µM
261 µM
593 µM
853 µM
1000 µM

Figure S2. Related to Figure 4.

(A) Overlay of [^{15}N-^{1}H]-BEST-TROSY spectra of free Taz2 (red) and Taz2 in complex with a 1.1 molar excess of p63 TA (green; p63 amino acids 1-34). Line broadening due to intermediate exchange is clearly visible on most peaks. Additionally, several unexpected peaks appear, indicating a non-homogenous sample.

(B) Assigned [^{15}N-^{1}H]- -BEST-TROSY of the optimized fusion construct between the p300 Taz2 and the TA of p63.

(C) TALOS based secondary structure prediction of a longer Taz2-p63 construct. Helical regions are shown in grey, sheet regions in blue and unfolded regions in orange. Due to the inability to sustain higher concentrations for an extended period of time only a partial assignment of this construct was possible. No further secondary structure was predicted C-terminal to amino acid P26.

(D) 2-step NMR titration of ^{15}N labeled p300 Taz2 with a two-fold excess of a p63 TA peptide spanning amino acids 8-21.

(E) 2-step NMR titration of ^{15}N labeled p300 Taz2 with a two-fold excess of a p63 TA peptide spanning amino acids 15-24.

(F) NMR titration of ^{15}N labeled p300 Taz2 with increasing molar ratios of p63 TA 8-32 ranging from 0 to 10-fold molar excess of peptide. The non-linear progression of the CSPs upon titration indicate a secondary binding event at higher excess of peptide.

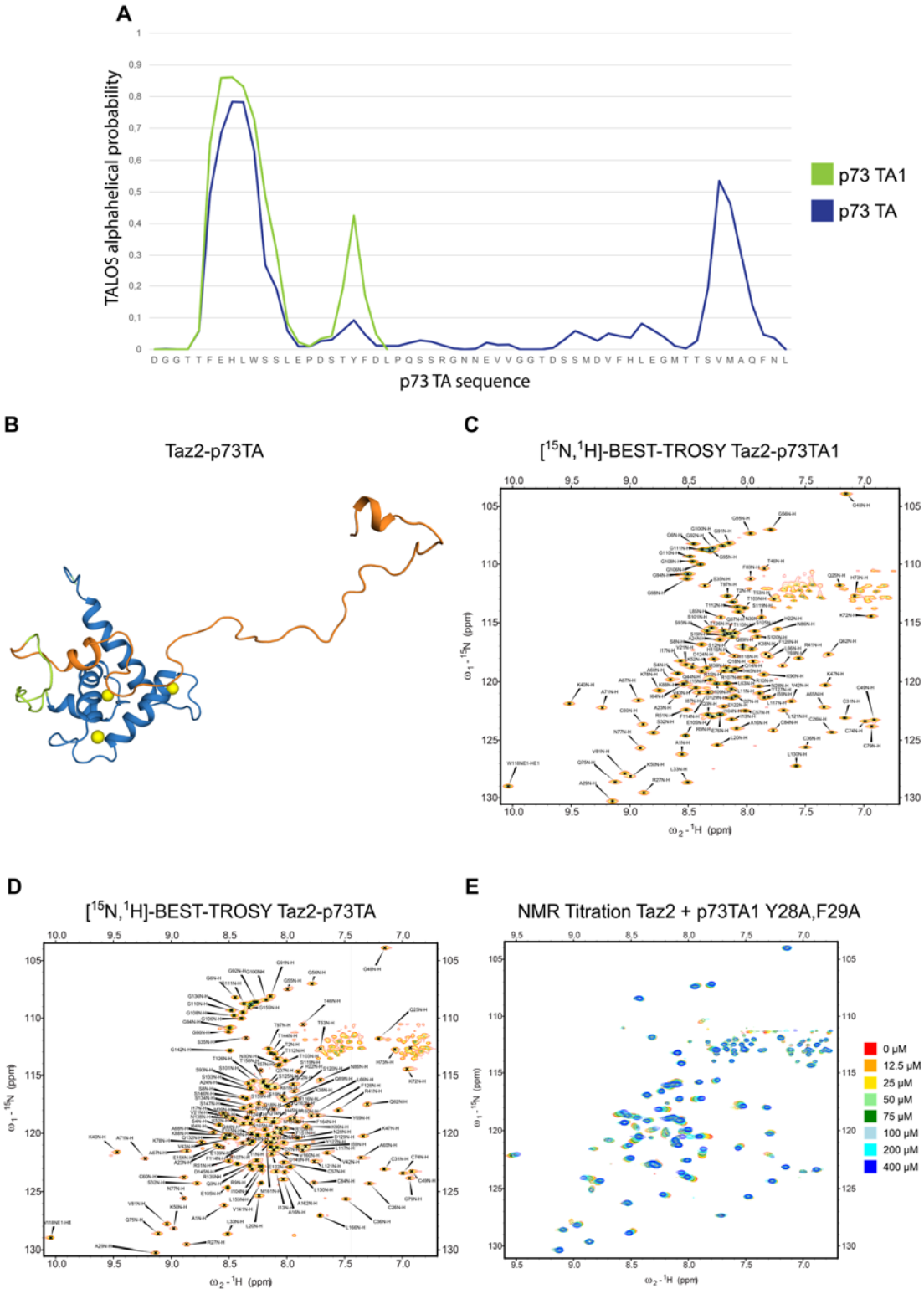

Figure S3. Related to Figure 4.

(A) TALOS secondary structure prediction based on the backbone assignment of p73 TA (blue) or p73 TA1 (green) in fusion constructs with p300 Taz2. Only the helical propensity of the corresponding peptide is plotted.

(B) Structure of the fusion construct of p300 Taz2 and the complete TA of p73. The overall peptide structure is almost identical to the short construct. An additional helix turn can

be observed between V61-F65. However, no assignable NOE contacts between this region and p300 Taz2 could be found, therefore the helix is not bound to the surface of Taz2.

(C) Assigned [^{15}N-^{1}H]-BEST-TROSY of the fusion construct between the p300 Taz2 and the TA1 of p73.

(D) Assigned [^{15}N-^{1}H] -BEST-TROSY of the fusion construct between the p300 Taz2 and the TA of p73.

(E) NMR titration of ^{15}N labeled p300 Taz2 with increasing molar ratios of p73 TA1 peptide (8-31; Y28A, F29A). Interaction can be observed, but the estimated K_D is >50 µM as saturation was not reached within the experiment.

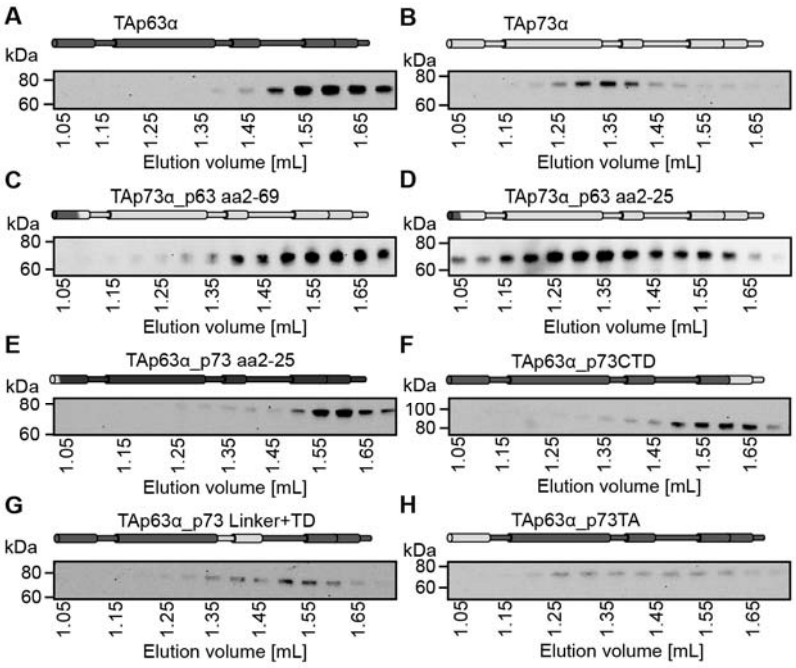

Figure S4. Related to Figure 5.

Western blot analysis of fractions (indicated as ml of elution volume) was performed for each chimera. The sum of all fractions was set to 100%. (A) TAp63α, (B) TAp73α, (C) TAp73α_p63 aa2-69, (D) TAp73α_p63 aa2-25, (E) TAp73α_p63 aa2-25, (F) TAp63α_p73CTD, (G) TAp63α_p73Linker+TD, (H) TAp63α_p73TA.